Energy harvesting: Energy harvesting with supercapacitor-based energy storage

Chapter · January 2015

DOI: 10.1007/978-3-319-14711-6_10

2 authors:

Sehwan Kim
Dankook University
79 PUBLICATIONS **1,008** CITATIONS
SEE PROFILE

Pai H. Chou
University of California, Irvine
218 PUBLICATIONS **4,657** CITATIONS
SEE PROFILE

Contents

Chapter 1
Energy Harvesting with Supercapacitor-Based Energy Storage

Sehwan Kim and Pai H. Chou

Abstract Harvesting energy from the environment is a desirable and increasingly important capability in several emerging applications of smart sensing systems. Due to the low-power characteristics of many smart-sensor systems, their energy harvesting systems (EHS) can achieve high efficiency by emphasizing low overhead in maximum power point tracking (MPPT) and the use of supercapacitors as a promising type of energy storage elements (ESE). Considerations in designing efficient charging circuitry for supercapacitors include leakage, residual energy, topology, energy density, and charge redistribution. This chapter first reviews ambient energy sources and their energy transducers for harvesting, followed by descriptions harvesters with low-overhead efficient charging circuitry and supercapacitor-based storage.

1.1 INTRODUCTION

Energy-harvesting smart sensing systems have been receiving growing attention in recent years. Smart sensing systems are those with autonomous control, communication, computation, and storage capabilities and are now used in a wide range of applications from wearable to environmental monitoring. Miniaturization, wireless communication, and high-capacity data storage capabilities open up new application domains by enabling a complete system to be mounted on or implanted inside many more physical objects than ever before. However, batteries need to be replaced or recharged, and they are often the most expensive part of the system. Although wire-

Pai H. Chou
University of California, Irvine, CA, 92697-2625 USA and National Tsing Hua University, Hsinchu, Taiwan, e-mail: phchou@uci.edu

Sehwan Kim
Dankook University, 119, Dandae-ro, Dongnam-gu, Cheonan-si, Chungnam, Republic of Korea
e-mail: paul.kim@dankook.ac.kr

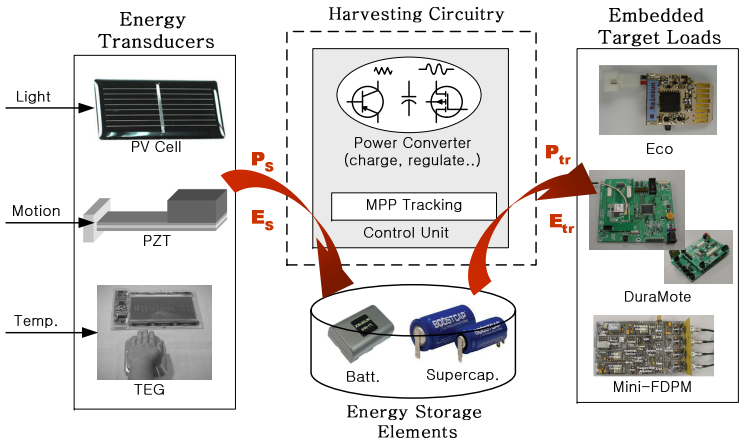

Fig. 1.1 The block diagram for EHS, powering smart sensing systems: Eco [31], DuraMote [18], and Mini-FDPM [32]

less communication makes it more flexible to deploy smart sensing systems at scale and can save expensive wiring cost, battery replacement can be even more costly if not prohibitive if the sensing nodes are deeply embedded. Utility power is not readily available at many deployment sites or remote locations, and energy harvesting is therefore mandatory in such cases.

However, anecdotes have often been about how costly and bulky these energy harvesters may be, how they fail to sustain days of poor weather, and how their batteries still fail after a year or two. The cost, size, and poor weather sustainability can be addressed by incorporating energy-harvesting circuitry that can extract the maximum amount of power from an energy transducer such as a solar panel over a wide range of supply conditions with low overhead. Several recent features that distinguish such harvesters from their utility-grade, larger counterparts include emphasis on *low overhead* in maximum power point tracking (MPPT) or maximum power transfer tracking (MPTT), and the use of *supercapacitors* as a potential type of energy storage elements (ESE) to address the problem of battery aging [4, 6, 14, 17, 37, 42].

Supercapacitors, also known as ultracapacitors or electrochemical double layer capacitors (EDLCs), have long life cycles and have been identified as a promising type of ESE for smart sensor nodes. In particular, supercapacitors and photovoltaic (PV) modules make an excellent combination for energy harvesters. This has motivated researchers to design efficient charging circuits for supercapacitors in their sensing systems. Supercapacitors have lower *energy density* than batteries do by an order of magnitude but much higher *power density*, which enables their use in applications that require short-term high power draw, such as electric vehicles and medical equipment [5, 32]. In particular, despite the lower energy density, their very long life cycles make them suitable for use as ESE for energy harvesting systems (EHS) [4, 6, 16, 37]. Such a system usually consists of the following four compo-

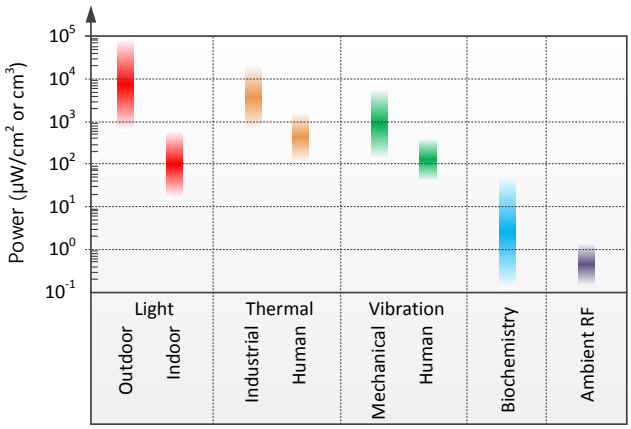

Fig. 1.2 Ambient sources power densities

nents: the energy transducers, (e.g., solar, wind, vibration etc.), energy-harvesting circuitry, energy storage subsystem, and target load, as shown in Fig. 1.1.

The main issues with EHSs for smart sensing systems are constraints on the form factor, harvesting efficiency, low-overhead harvesting circuitry, scalability to multiple reservoirs, and cold booting control. To solve these issues, each of the subsystems may be optimized in isolation, but together they can be jointly optimized with interesting trade-offs. Therefore, it is critical to devise (1) charging circuits to maximize harvesting efficiency and (2) the circuits to automatically find the maximum power point (MPP). Furthermore, supercapacitors-based energy storage subsystem should consider the nonlinearity of supercapacitors such as leakage, residual energy, topology, energy density, and charge redistribution to charge the supercapacitors efficiently. As a result, supercapacitor-based energy-harvesting smart sensing systems can lead to several benefits including cost effectiveness, small form factor, and long operating lifetime.

The chapter is organized as follows: In Section 1.2, energy transducers are modeled with an examination of their MPP. Section 1.3 describes techniques for maximizing the efficiency of energy harvesters, and Section 1.4 takes a close look at supercapacitor-based energy storage subsystems. Finally, Section 1.5 presents a summary of this chapter.

1.2 ENERGY TRANSDUCERS

Ambient energy sources are often available in the surroundings of most deployment sites. Examples of such energy sources include mechanical (vibrations, deformations), thermal (temperature gradients or variations), radiant (sun, infrared, RF), and

chemical energy (chemistry, biochemistry) sources. They are characterized by different power densities as shown in Fig. 1.2. Energy harvesting from the sun is the most powerful but is not always available or efficient under low solar irradiation conditions such as poor weather or dark places. Similarly, it is not possible to harvest energy from thermal sources where there is no thermal gradient or to harvest vibration energy where there is no vibration. As a consequence, the source of ambient energy must be chosen according to the deployed environment of the smart sensor nodes.

Each given source of ambient energy can be converted by a different energy transducer that performs conversion to electrical energy. To the system, the key differences of energy transducers are the output power level, alternating current (AC) vs. direct current (DC), the dynamic range, and the impedance model. For instance, Fig. 1.2 shows that 10$\sim$100 μW of available output power level is a good order of magnitude for a 1 cm^2 or a 1 cm^3 energy transducer. Although 10$\sim$100μW may not be a great amount of power, it can be enough for many applications of smart sensor systems. Of the different types of transducers, windmills [22], magnetic coil generators [24], piezoelectric generators [2, 28, 35], and magnetic induction [7] output AC power, whereas thermal [1] and photovoltaic [14, 34, 37] power sources output DC power.

Maximum power point tracking (MPPT) refers to drawing power from these energy transducers at a level that maximizes the power output. Furthermore, maximum power transfer tracking (MPTT) attempts to find actual MPP by considering the efficiency of harvesting circuitry. Therefore, although there has been extensive research from the device perspective to improve the cost, conversion efficiency, and power density of transducers, it is crucial for system designers to understand their electrical characteristics in-depth in order to analyze their impact on the system being powered. Therefore, in this section, the maximum power point (MPP) of each energy transducer depending on the output power is described with the equivalent circuit models of the energy transducers. The electrical equivalent-circuit model is important for validation by simulation and optimization of the harvester at the system level.

1.2.1 Direct Current Electricity

This section introduces photovoltaic transducers as a representative type of DC output power sources by describing its characteristics through the equivalent circuit models.

Photovoltaic Cells: Photovoltaic (PV) cells are the most well-known type of DC-power source for its high power density. Fig. 3(a) shows the equivalent circuit of a solar cell, which can be modeled as a current source with a voltage limiter. Based on the circuit, the output current (I_{pv}) of a solar cell can be expressed as:

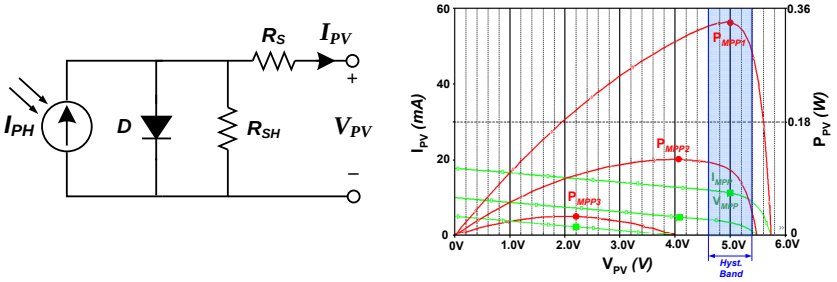

(a) Solar cell circuit model

(b) *I-V* (green) / *P-V* (red) Characteristics and Hysteresis Window of MPP

Fig. 1.3 The Characteristics of a Solar Cell

$$I_{\mathrm{pv}} = I_{\mathrm{ph}} - I_{\mathrm{o}} \left(e^{q \frac{V_{\mathrm{pv}} + I_{\mathrm{pv}} R_{\mathrm{s}}}{A k T_{\mathrm{STC}}}} - 1 \right) - \frac{V_{\mathrm{pv}} + I_{\mathrm{pv}} R_{\mathrm{s}}}{R_{\mathrm{sh}}} \tag{1.1}$$

where I_{o} is the reverse saturation current, q is the electron charge, A is the diode quality factor, k is the Boltzmann constant, T_{STC} is the operating temperature at Standard Test Conditions (STC), for which the irradiation is 1000 W/m^2 and the panel temperature (T_C) is 25°C, and R_{s} and R_{sh} are the panel series resistance and panel shunt resistance, respectively.

Fig. 3(b) shows the simulation result for a solar panel using Eq. (1.1). The panel parameters were extracted by previous work [36]. The power output of the solar panel is not constant but has a wide dynamic range due to the many intensity levels of sunlight. Moreover, the P_{MPP3} indicates the P-V curve under the low solar irradiation condition in the morning, in the evening, or on cloudy days. In such conditions, the solar cell's voltage may be too low to operate the target system or charge up the ESE, and therefore this energy can be wasted, unless the voltage is boosted up.

Thermoelectric Generators: Thermoelectric generators (TEGs) convert geothermal energy into electrical energy by the Seebeck effect. The TEG has not become widespread yet because of the low conversion efficiency. Despite the low efficiency of the TEGs, the prospect of thermoelectric power generation has rapidly become very promising with the growing public interest in environmental problems in recent years. By using differing combinations of series and parallel connections of the junction pairs, the output voltage and current of the harvester can be adjusted. Typically, a series connection is used to maximize the output voltage, at the expense of current, to reach a usable voltage level at lower temperature gradients.

The basic equivalent circuit of a TEG is illustrated in Fig. 4(a), which is modeled the generation voltage source V_{G} and the internal resistor R_{in}. The open-circuit voltage (V_{oc}) of the TEG is expressed as:

$$V_{\mathrm{oc}} = N(\alpha_{\mathrm{p}} - \alpha_{\mathrm{n}})(T_{\mathrm{H}} - T_{\mathrm{C}}) \tag{1.2}$$

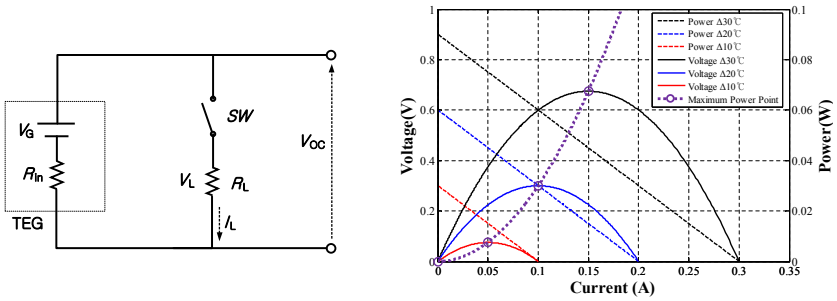

(a) TEG circuit model (b) *V-I* / *P-I* Characteristics and MPP of a TEG

Fig. 1.4 The Characteristics of a TEG

where α_{p} and α_{n} are the Seeback coefficients of *n*-type and *p*-type material, respectively. N is the number of thermoelements. $(T_{\mathrm{H}} - T_{\mathrm{C}})$ is temperature difference between hot side and cold side of the TEG. According to Eq. (1.2), the open circuit voltage (V_{OC}) of the TEG is directly proportional with the number of thermoelements and the temperature gradients [3].

The output power $P_{\mathrm{out,TEG}}$ in this circuit can be given by:

$$P_{\mathrm{out,TEG}} = I_{\mathrm{L}} V_{\mathrm{L}} = I_{\mathrm{L}}(\alpha \Delta T - I_{\mathrm{L}} R_{\mathrm{in}}) = \alpha^2 \Delta T^2 \frac{R_{\mathrm{L}}}{R_{\mathrm{in}} + R_{\mathrm{L}}}, \tag{1.3}$$

where P_{out} is the output power, I_{L} is the electric current flowing through the load, V_{L} is the generated voltage on the load by the TEG, ΔT is the temperature difference between hot side and cold side, R_{in} is the TEG electrical resistance, and R_{L} is the TEG load resistance.

The power transfer is maximized when the impedance is matched, i.e., the load resistor R_{L} is equal to the TEG internal resistor R_{in}. This load condition is given by [12, 15]:

$$P_{\mathrm{out,TEG}}^{\max} = \frac{\alpha^2 \Delta T^2}{4 R_{\mathrm{in}}}. \tag{1.4}$$

Using Eqs. (1.3) and (1.4), the voltage-current and power characteristics of a TEG can be plotted as shown in Fig. 4(b).

When the temperature difference between the surfaces of TEG is changed, the output voltage of the TEG varies accordingly. However, most loads to be powered require a standard supply voltage, which can be produced by DC-DC converters. Otherwise, TEGs are connected in series and in parallel to achieve sufficient power.

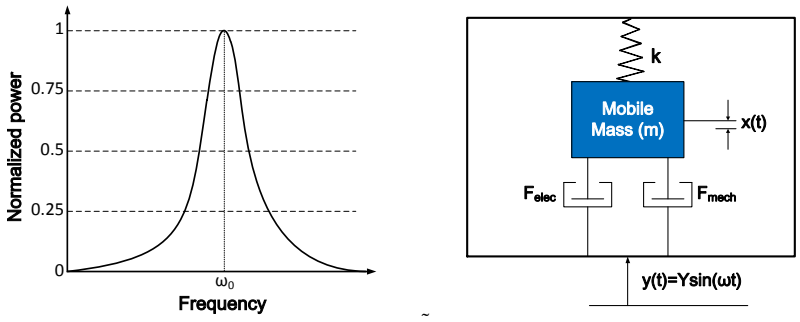

(a) Resonance phenomenon (b) Equivalent model

Fig. 1.5 Vibration Energy Harvesters

1.2.2 Alternating Current Electricity

Mechanical energy is possibly the most prevalent AC-output power source and are found in windmills [22], magnetic coil generators [24], piezoelectric generators [2, 28, 35], and magnetic induction [7], and many more. Among them, in this section, we focus on the vibration-powered generators as AC-output transducers. Vibration energy harvesting is to convert vibrations into electrical power. Actually, turning ambient vibrations into electricity is a two-step conversion process: vibrations are first converted in a relative motion between two elements, thanks to a mass-spring system, that is then converted into electricity by a mechanical-to-electrical converter (e.g., piezoelectric material, magnet-coil, or variable capacitor). As ambient vibrations are generally low in amplitude, when the mass-spring system is in resonance, the relative movement amplitude of the mobile mass is amplified compared to the vibrations amplitude, thereby increasing the harvested power as shown in Fig. 5(a). The resonance point can be a maximum power point of the vibration-powered generators.

Fig. 5(b) represents the equivalent model of vibration harvesters. A mass (m) is suspended in a frame by a spring (k) and damped by forces (f_{elec} and f_{mec}). When a vibration occurs $y(t) = Y\sin(\omega t)$, it induces a relative motion of the mobile mass $x(t) = X\sin(\omega t)$ compared to the frame. A part of the kinetic energy of the moving mass is converted into electricity (modeled by an electromechanical force f_{elec}), while another part is lost in friction forces (modeled by f_{mec}). The maximum output power of a resonant energy harvester submitted to an ambient vibration is reached when the natural angular frequency (ω_0) of the mass-spring system is equal to the angular frequency of ambient vibrations (ω) and when the damping rate $\xi_m = b_m/(2m\omega_0)$ of the mechanical friction force f_{mec}. The maximum power point can be expressed as

$$P_{\text{out, vib}}^{\max} = \frac{mY^2\,\omega_0^3\,Q_m}{8}. \tag{1.5}$$

To induce this electromechanical force, it is necessary to develop a mechanical-to-electrical converter to extract a part of mechanical energy from the mass and to turn it into electricity [38].

Three main types of devices that convert mechanical energy into electricity are piezoelectric, electromagnetic, and electrostatic generators, as shown in Fig. 1.6. Piezoelectric ones employ active materials that generate a charge when mechanically stressed or strained. Electromagnetic generators are based on electromagnetic induction arising from the relative motion between a magnetic flux gradient and a conductor. Electrostatic generators use a variable capacitor structure to generate charges from a relative motion between two plates. Detailed explanations for the three main types of devices are as follows.

Piezoelectric generators: Piezoelectric ceramics have been used for many years to convert mechanical energy into electrical energy. In particular, the use of piezoelectric generators to power human-wearable systems has been extensively studied because of their higher output voltages, high capacitances, and no need to control any gap. Human motion can be characterized by large-amplitude movements at low frequencies, and therefore it is difficult to design a miniature resonant generator to work on humans. Coupling by direct straining of, or impacting on, piezoelectric elements have been applied to human-wearable systems. A subsequent device has been developed [23] by mounting an 8-layer stack of PVDF laminated with electrodes on either side of a 2 mm-thick plastic sheet. This stave was used as an insole in a sports training shoe. At a frequency of a footfall of 0.9 Hz, this arrangement produced an average power of 1.3 mW into a 250 kΩ load.

Electromagnetic generators: Electromagnetic induction is the generation of electric current in a conductor located within a magnetic field. The conductor typically takes the form of a coil and the electricity is generated by either the relative movement of the magnet and coil or by changes in the magnetic field. One of the most effective methods for energy harvesting is to produce electromagnetic induction by means of permanent magnets, a coil, and a resonating cantilever beam.

Several companies specializing in the field of energy harvesting have emerged over recent years. A shake flashlight or faraday flashlight uses the electromagnetic generator. During shaking, a magnet passes back and forth through a coil of wire and creates an electrical current that is then stored in a supercapacitor or battery. When the flashlight is turned on, the capacitor supplies the stored energy to the bulb. Besides flashlights, micro generating systems have also been developed for watches [20].

Electrostatic generators: Electrostatic generators are capacitive structures made of two plates separated by air, vacuum, or any dielectric materials. A relative movement between the two plates generates a capacitance variation and then electric charges. These electrostatic generators can be divided into electret-free and electret-based ones. The former uses conversion cycles made of charges and discharges of

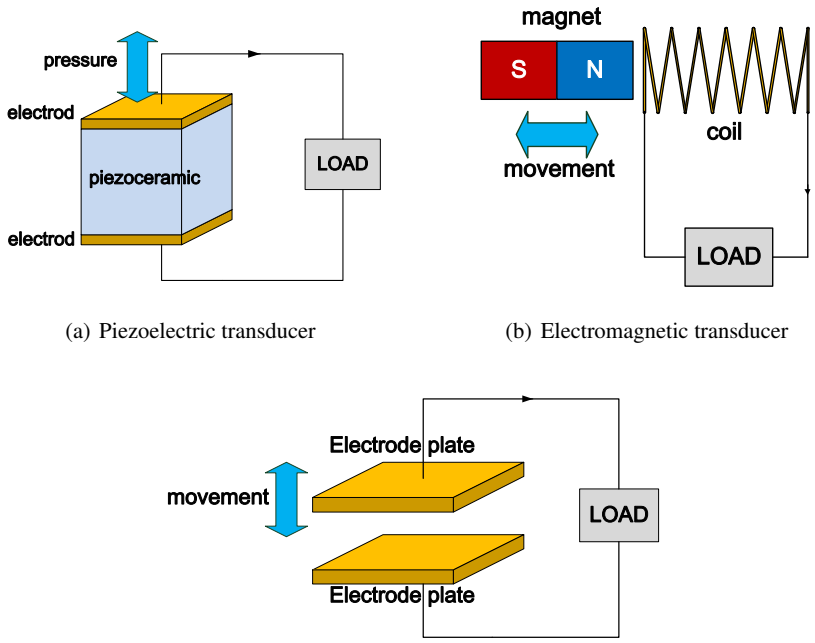

(a) Piezoelectric transducer

(b) Electromagnetic transducer

(c) Electrostatic transducer

Fig. 1.6 Mechanical-to-electrical conversion for smart sensor systems

the capacitor while the latter uses electrets, giving them the ability to directly convert mechanical power into electricity.

An electrostatic generator is well-adapted for size reduction, increasing electric fields, and capacitances. It can also offer the possibility to decouple the mechanical structure and the generator. Finally, it enables development of low-cost devices as they do not need any magnet or potentially expensive piezoelectric material.

1.3 TECHNIQUES FOR MAXIMIZING EFFICIENCY OF HARVESTERS

Energy harvesters for smart sensing systems can achieve efficient operations through tracking the maximum power point. This section first provides the basic principle of MPPT on energy transducers, specifically solar cells, in terms of an equivalent circuit model. Next, it presents approaches to MPPT and describes techniques for maximizing the efficiency of energy harvesters at subwatt scale, followed by a comparison of MPTT issues.

1.3.1 Maximum Power Point Tracking

The MPP of an energy transducer changes with the strength of the ambient energy source as shown in Fig. 3(b). The purpose of *maximum power point tracking* (MPPT) is to track the supply condition and determine the corresponding load that maximizes the transferred power, namely operating at the MPP. The most significant design consideration for MPP tracking in subwatt-harvesters is to ensure that MPP tracking incurs minimal power overhead, as the output power from the energy transducer is very limited.

Graphical Load-Line Analysis: A solar panel consists of a matrix of solar cells, also known as photovoltaic (PV) cells. This section explains how a solar panel works in terms of a circuit model. Fig. 7(a) shows the equivalent circuit model of a solar cell. It can be described as one ideal current source and a voltage limiter, as shown in Fig. 7(a), where I_O is proportional to the sunlight intensity. Therefore, one of the most important issues for a solar cell is how to efficiently deliver as much power to the load (represented by R_L) as possible for a given I_O, as determined by a given level of sunlight intensity.

Fig. 7(b) illustrates MPPT by graphical load-line (represented by R_{L}) analysis, with the assumption that I_{O} increases gradually. When I_{O} is small, most I_{O} will flow to R_{L}, because the diode does not turn on before reaching 0.7 V. As I_{O} increases, V_{L} will eventually approach 0.7 V, and the diode turns on. As a result, any additional increase of I_{O} will result in current flowing to the diode instead of the load. Thus, at high I_{O}, V_{L} is approximately 0.7 V and I_{L} is saturated at $0.7/R_{\mathrm{L}}$. Therefore,

$$I_{\mathrm{S}} = I_{\mathrm{O}} - I_{\mathrm{D}} \tag{1.6}$$

$$I_{\mathrm{L}} = V/R_{\mathrm{L}} \tag{1.7}$$

The solution for $I_{\mathrm{S}} = I_{\mathrm{L}}$ and V can be found by plotting I_{S} and I_{L} separately vs. V as shown in Fig. 7(b). By graphical load-line analysis, the solution for $I_{\mathrm{S}} = I_{\mathrm{L}}$ and V changes from (1) to (2) and (3) as I_{O} increases. After approaching the point (3), any further increment in I_{O} will not affect the power conversion efficiency. At this point, one can increase the power conversion efficiency only by lowering R_{L}, because the slope of the load line is inversely proportional to R_{L}. In detail, the shaded area of Fig. 7(b) is equal to harvested power that is transferred to the load. Comparing the three load-resistor values $R_{\mathrm{L}1}$, $R_{\mathrm{L}2}$, and $R_{\mathrm{L}3}$, $R_{\mathrm{L}2}$ results in the maximum power conversion when the "diode" is just turned on. This analysis result shows that adjusting the slope of the load line is the pivotal parameter for transferring the maximum power from the solar cell to the load. The saturation voltage V_{D} can be increased beyond 0.7 V by series and parallel compositions of the solar cells.

Since MPPT overhead is potentially high, many energy harvesters for smart sensor systems have not performed MPPT until recent years. These MPP trackers must consider the net amount of power that can be transferred, i.e., after the MPPT overhead has been subtracted. One common approach is to sacrifice MPPT optimality for significantly reduced overhead. That is, by harvesting within, say, 5-10% from

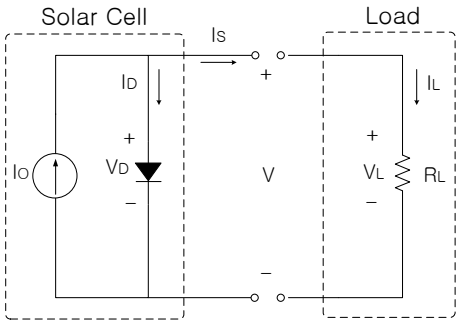

(a) Equivalent Circuit Model of Solar Cell.

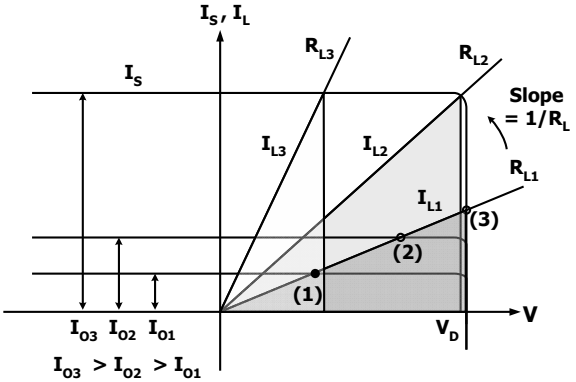

(b) *I-V* curve and load lines of a Solar Cell.

Fig. 1.7 The basic of MPPT at a solar cell

the MPP, one may cut down on the MPPT overhead significantly, which may result in much higher net power. One way to classify MPPT approaches is consumption side vs. supply side. Consumption side is represented by load matching, while supply side is further divided into sensor-driven and perturbation-based MPPT.

Load Matching: A consumption-side subwatt-solar MPPT approach is called *load matching*, which means to adjust the load directly to maximize the utility of power when available. The load can be adjusted by duty cycling or *dynamic power management* (DPM), among many techniques published in the low-power literature. One reason for maximizing power utility is to minimize power loss due to conversion and energy loss due to storage [9, 29], although one can always store the excess power as yet another form of load.

Actually, load matching is a special case of *load following*, where the duty cycling [11] or DPM [42] tracks the level of available power (e.g., based on a light sensor) without necessarily tracking the MPP (i.e., transferred power). Because load

following does not necessarily track the MPP, it can actually lead to system failure if there is no energy storage, because overloading the solar panel will result in lower transferred power than the peak load. Another consideration is that both load matching and load following tend to be application specific.

Sensor-driven MPPT: With sensor-driven MPPT, a sensor is used to measure the intensity of the ambient power, which is the primary parameter that determines the MPP. For instance, the MPP for a solar panel is primarily determined by the light intensity, and the MPP for a wind generator is primarily determined by the rotational speed of the fan. The sensor value can then be used to determine the load that will result in the MPP. The use of a sensor does not require perturbation to the energy harvesting source and enables very simple circuitry to be built, such as the case with AmbiMax [30]. In fact, AmbiMax can also take a rotational speed sensor for a wind generator. However, a sensor itself may consume power. One alternative that addresses this problem, at least for the solar part, is to use a *pilot cell*, which is a miniature PV cell that outputs its harvested power instead of consuming power [4]. A small pilot cell can be made in about the same size as a photo sensor.

In both cases, however, under partial shading conditions, either the photo sensor or the pilot cell may fail to output a representative value for the solar panel's exposure to solar power. A related problem is aging and other forms of deterioration, where even without partial shading, the photo sensor or the pilot cell's output is no longer a good indicator of the MPP. In the latter cases, the energy harvesting system would need to be re-calibrated.

Perturbation-based MPPT Perturbation-based MPPT [13, 25, 39] approaches do not rely on sensors to measure the ambient power level in order to derive the MPP; instead, they test the generator itself to determine the MPP. Such MPPT approaches include open-circuit voltage, short-circuit current, hill climbing, and *I-V* curve sweeping.

Open-circuit voltage (V_{oc}) and *short-circuit current* (I_{sc}) approaches use V_{oc} and I_{sc} to determine the ambient power level, respectively [27]. This can be viewed as using the entire solar panel as a sensor. However, the price to pay is that it requires the load to be disconnected momentarily while the V_{oc} or I_{sc} is measured. One may approximate the V_{mp} or I_{mp} as a linear function of V_{oc} or I_{sc}, respectively:

$$V_{\text{mp}} = k_1 V_{oc} \tag{1.8}$$

$$I_{\text{mp}} = k_2 I_{sc} \tag{1.9}$$

where k_1, k_2 are proportional constants.

Once k_1 and k_2 are known, I_{sc} can be simply measured by shorting the solar cell using periodic switching operation, and V_{oc} also can be measured periodically by momentarily shutting down the power converter. To handle the temporary loss of power while measuring V_{oc} or I_{sc}, some circuitry such as a capacitor is required to power the rest of the system briefly. The accuracy of V_{mp} and I_{mp} depends on the constants k_1, k_2.

A more accurate method is called hill-climbing, where perturbing the duty ratio of the power converter perturbs the solar panel's current and consequently perturbs the solar panel's voltage [21]. On the *P-V* curve, if the output power increases in response to increasing (or decreasing) duty ratio, then the MPP tracker continues generating perturbation with incremented (or decremented) duty ratio; but if the power decreases, then the subsequent perturbation should be reversed. The system then oscillates about the MPP. The oscillation can be minimized by reducing the perturbation step size. However, a smaller perturbation size slows down the convergence speed of MPPT. In this sense, even though hill-climbing is more accurate, it has the drawback that the convergence speed is unstable depending on the perturbation step size. Hill-climbing tracks two points in order to find the MPP, and thus it consumes more power than V_{oc} or I_{sc} method.

I-V curve sweeping is an even more precise MPPT approach, which measures the *I-V* characteristic of the solar panel by varying a test load. Note that all other approaches also need to rely on some characterization of the solar panel, also done by sweeping the *I-V* curve, except that they are done before deployment. The advantages to doing *I-V* curve sweeping at runtime are that (1) it tracks the exact characteristics of the solar panel over time, even as it ages or becomes dusty, (2) the same MPPT logic can work with a wide range of replacement solar panels automatically, without requiring the user to manually characterize each one and updating the control parameters. As with other perturbation-based MPPT techniques, *I-V* curve sweeping at runtime also requires the system to be disconnected from the solar panel momentarily. It may incur slightly more cost, but in practice, the cost is only slightly higher than other simpler perturbation-based MPPT approaches.

1.3.2 Maximum Power Transfer Tracking

The MPP found by conventional trackers that consider only the energy transducer can be quite different from the MPP at the *system level* when taking the efficiency of the charging circuitry into account. To address this problem, maximum power transfer tracking (MPTT) has been proposed.

The impact of charging-circuit efficiency on MPP: To maximize the amount of energy stored in the supercapacitor, we should maximize $P_{\text{charge}} = \eta \cdot P_{\text{pv}}$. Indeed, conventional MPPT methods maximize P_{pv} with the expectation that P_{charge} is also maximized. However, MPPT without considering the charger efficiency may result in low transferred power, as shown in Fig. 8(a). Because the charging circuit efficiency η is varying depending on output current (I_{out}), conventional MPPT techniques cannot guarantee that the maximum P_{ambi} is equal to the maximum P_{scap}, unless the charging circuit's efficiency for the EHS is also taken into account.

Fig. 8(b) shows that MPP_{solar} (marked by squares) is shifted to MPP_{scap} (marked by circles) after power passes through the charging circuit of the harvesting system.

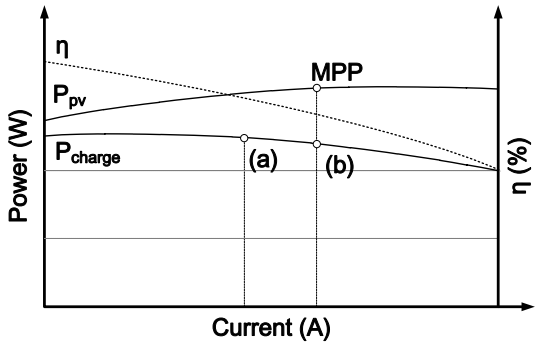

(a) MPP is shifted due to efficiency (η) varies. $P_{\text{charge}} = \eta \cdot P_{\text{pv}}$.

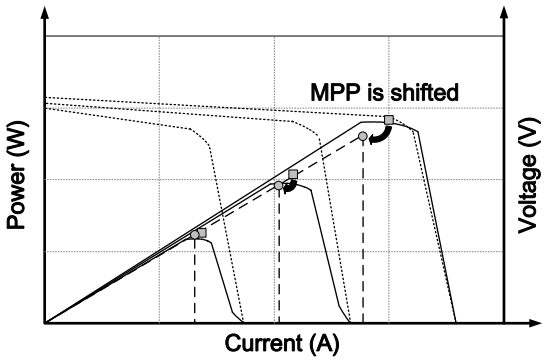

(b) MPP_{scap} vs. MPP_{solar}, when $P_{scap} = \eta \cdot P_{abmi}$.

Fig. 1.8 The shift of MPP at a solar cell depending on solar intensity

The amount of shift is linearly proportional to the output current I_{out}. For instance, at 1000 W/m^2, we can see a significant drift from MPP_{solar} to MPP_{scap}.

Maximum Power Transfer Tracking: To address this problem, maximum power *transfer* tracking (MPTT) was proposed to consider the efficiency of the charging circuits as a function of the load [19]. To realize MPTT, the efficiency range of charging circuits needs to be considered; thus, the MPPT circuitry should be placed right before the supercapacitors to implement a more accurate MPP tracker. A novel charging circuit with MPTT using a charge pump to charge supercapacitors was proposed in [16]. Its four primary tasks are (1) sensing the current from the ambient power source(s) and selecting the suitable input capacitance C_{in}, (2) sweeping the switching frequency and tracking I_{MPP} using the *I-F* curve, (3) feeding the microcontroller unit (MCU) the maximum power transfer point (MPTP) and reconfiguring the smart switch array to optimize the input capacitors or connect the reservoir su-

percapacitors in series or as single cells, and (4) charging the selected supercapacitor with I_{MPP}.

MPP trackers vs. MPTP trackers: MPPT techniques described above can be realized using commercial off-the-shelf components that supported hysteretic control. For example, one popular component for MPP trackers such as [4,6,30] is LTC1440, an ultra-low power comparator from Linear Technology. It supports programmable lower and upper bounds of the hysteresis band as indicated by the shaded region in Fig. 3(b). In this way, the actual operating point of the MPP tracker oscillates around the MPP, rather than being a fixed point. By tuning to a narrow hysteresis band, this can lead to higher efficiency of the power converter, but it may not be able to match the dynamic range of the ambient power conditions, making the MPP tracker operate at an inefficient level. Taking PV cells as an example, in the early morning, the solar irradiation intensity can be very low such that the MPP tracker with a narrow tuning hysteresis band fails to properly track the maximum power point as shown in Fig. 3(b).

On the other hand, the MPTP tracker in [16] was designed by using a frequency sweeper. Since the frequency sweeping range of a charge pump is directly related to the wide dynamic range of various ambient power sources, a direct digital synthesizer (DDS) was employed to cover the wide dynamic range of the charging circuit. Although it is possible to cover this wide frequency range using multiple analog oscillators, doing so will increase the system complexity and induce higher overall power consumption. For this reason, a DDS can be the best candidate for the charge pump as a substitute for a conventional analog oscillator. A commercially available DDS chip, AD9834, can generate frequencies from 0 to around 40 MHz with power overhead of around 18 mW.

Harvesting Threshold Although an MPTT charger can convert power efficiently over different levels of ambient power, it is unable to actually charge the ESE when the converted power is below a threshold. Some MPPT and MPTT chargers have relatively high thresholds, because they are unable to cover the wide dynamic range of the ambient power source. Therefore, when below the threshold, the charging efficiency is not the *conversion efficiency* of the circuity, but is 0% because of zero charging activity. A charger with a higher threshold is said to have a narrower *charging zone* than one with a lower threshold. The overall efficiency of a harvester therefore must consider not only the efficiency of the conversion circuitry but also scale it by the width of its charging zone.

A harvester with high conversion efficiency but a narrow charging zone may be suitable for scenarios with plentiful ambient power. However, it may fail to sustain consecutive days of poor weather or areas with greater seasonal variations of sunlight availability. A common solution to this problem is to *over-design* the system by incorporating a much larger solar panel than necessary, but this can increase the cost significantly. One particular reason for a narrow charging zone in previous designs is the use of buck-type charging circuits [4, 6, 37]. They convert the power from the solar panel down to a lower voltage, and this effectively sets the threshold to a potentially high level (and therefore narrows the charging zone). A buck-boost

converter can be used as a general solution, especially for rechargeable batteries. However, they may not be able to handle the wide dynamic range of solar panels. Moreover, both buck and buck-boost converters require the use of an inductor as a low pass filter (LPF), which increases the size of the harvesters, as the inductor tends to be bulky. To address this problem, a charge pump may be a better solution, as it does not require additional inductors and thus can be made smaller, and it also supports a much wider dynamic range [16]. It is also particularly suitable supercapacitor-based storage, which can be charged as long as the charging voltage is higher than the supercapacitor's voltage, rather than requiring a fixed target voltage. This can significantly reduce the harvesting threshold.

1.4 ENERGY STORAGE SUBSYSTEMS

Batteries are the primary type of power source for smart sensing systems. Among rechargeable batteries, Li-ion and Li-polymer batteries have the highest energy density and high charge-to-discharge efficiency. Charging of a lithium-type battery is more complicated and is usually handled by a charging IC. Several works cited this reason and chose nickel metal hydride (NiMH) batteries instead. NiMH is one of the most popular types of energy storage for its relatively high energy density and relatively simple charging method, i.e., trickle charging. Nickel-Cadmium (NiCd) batteries have the advantage of higher discharge rates and can tolerate deeper discharge cycles than lithium batteries can. However, in practice, they can suffer from the *memory effect*, or an apparent loss of capacity if it is recharged before being fully discharged. Rechargeable batteries also have a limited number of recharge cycles on the order of 1000.

Thanks to long charging-discharging life cycles, supercapacitors have been receiving growing interest as energy storage in addition to or instead of batteries in a new generation of energy harvesters. Table 1.1 shows a comparison between batteries and supercapacitors. Although its capacity is still much smaller than other types of batteries, a supercapacitor can store enough energy to power many smart sensor systems.

Table 1.1 Comparison between Batteries and Supercapacitors

	Battery	Supercapacitor
Recharge Cycle Life Time	$< 10^3$ cycles	$> 10^6$ cycles
Self-discharge Rate	5%	30%
Voltage	3.7V-4.2V	0V-2.7V
Energy Density (Wh/kg)	high (20-150)	low (0.8-10)
Power Density (W/kg)	low (50-300)	high (500-400)
Fastest charging time	hours	sec $\sim$ min
Fastest discharging time	0.3$\sim$3 hours	$<$ a few min
Charging Circuit	complex	simple

In particular, its relatively high maximum recharging cycle life time allows it to be used for long-lifetime applications.

1.4.1 Supercapacitors in Sub-Watt Energy Harvesters

Supercapacitors have high power density, but they cannot be used as drop-in replacements for batteries without considering their intrinsic characteristics such as the discharge (voltage-vs.-energy) curve, leakage, charge redistribution, residual energy, energy density, topology, and cold booting. Their voltage depends on the amount of stored energy, and they work as a virtual short circuit during charging phase. Moreover, supercapacitors have higher leakage current than rechargeable batteries do.

To address the issues and improve the charging efficiency of supercapacitors in sub-watt energy harvesters, researchers have used buck, boost, or buck-boost dc-dc converters in conjunction with control logic circuitry [4, 37, 41]. The control logic circuitry plays a pivotal role in increasing the charging efficiency of supercapacitors by tracking the MPP. Researchers have developed MPP-tracking supercapacitors-charging circuitry using dc-dc converters, and many assume solar sources with high power density under strong sunlight, but it is challenging to charge supercapacitors efficiently with low-overhead MPPT circuitry. Therefore, it is important to first identify the nonideality of supercapacitors and consider it at design time to improve efficiency of supercapacitor charging circuitry.

1.4.2 The Characteristics of Supercapacitors

Equivalent circuit model of supercapacitors: Many circuits-based supercapacitor models have been proposed to simulate the various characteristics of supercapacitors [10, 33, 40]. This section describes two equivalent circuit models: (1) an *R-C equivalent circuit model*, which is suited for the relatively low energy flow and the long time aspects during charging and discharging; (2) the variable leakage resistance model for analysis of charge redistribution of supercapacitors and power management research.

The R-C equivalent circuit model is composed of three components: the equivalent serial resistance $R_{\text{esr,scap}}$, the equivalent parallel resistance $R_{\text{epr,scap}}$, and the capacitor C_{scap}, as shown in Fig. 9(a). The $R_{\text{esr,scap}}$ is the internal series resistance, which represents losses in charging or discharging cycles. The $R_{\text{epr,scap}}$ is connected in parallel with the capacitor. The $R_{\text{epr,scap}}$ is used to model the leakage current loss that represents long-term storage characteristics. Differing from the R-C equivalent circuit model, the *variable leakage resistance model* features two resistor-capacitor branches. The capacitor in the first branch includes a constant capacitor C_a and a voltage dependent capacitor C_v. The other branch consists of a constant capacitor

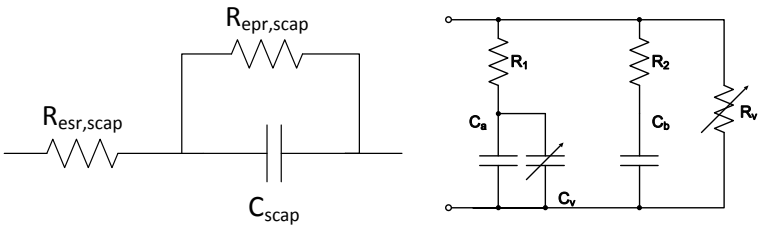

(a) R-C circuit model (b) Variable Leakage Resistance model

Fig. 1.9 Equivalent Circuit Model of Supercapacitors

C_b. The variable resistor R_v is related to self discharge. The rated voltage V_{nom} denotes the highest voltage to which the supercapacitor can be charged.

Leakage: Given the initial voltage V_0, when the positive and negative terminals of the supercapacitor are opened, the voltage drop due to $R_{\text{epr,scap}}$ is a decay of the initial voltage V_0. Thus,

$$V_{\text{scap}}(t) = V_0 e^{-\frac{t}{R_{\text{epr,scap}} C_{\text{scap}}}} \tag{1.10}$$

During a particular time, from t_{start} to t_{end}, the leakage energy of the supercapacitor can be expressed as

$$E_{\text{leak,scap}} = 0.5\, C_{\text{scap}} (V^2_{\text{scap}}(t_{\text{start}}) - V^2_{\text{scap}}(t_{\text{end}})) \tag{1.11}$$

$$= \int_{t_{\text{start}}}^{t_{\text{end}}} \frac{V^2_{\text{scap}}(t)}{R_{\text{epr,scap}}} dt \tag{1.12}$$

According to Ohm's Law, the leakage current can be written as

$$I_{\text{leak,scap}}(t) = \frac{V_{\text{scap}}(t)}{R_{\text{epr,scap}}} \tag{1.13}$$

As the capacitance of a supercapacitor increases, its leakage current also increases, while $R_{\text{epr,scap}}$ decreases. In addition, when the voltage of the supercapacitor rises, the leakage current gradually increases; that is, it is proportional to the charged voltage of the supercapacitor. To charge the supercapacitor with a low ambient-power source, the charging power should be higher than the leakage power. Therefore, the power-transfer efficiency of a dc-dc converter and the additional overhead of the control circuit are crucial factors in determining the efficiency of the charger for supercapacitors. Fig. 1.10 shows the characteristic of the leakage current depending on the charged voltage of the supercapacitor.

The measured leakage current is marked by asterisks for a 25 F supercapacitor and indicated by squares for an 1 F supercapacitor. By fitting of the measured results

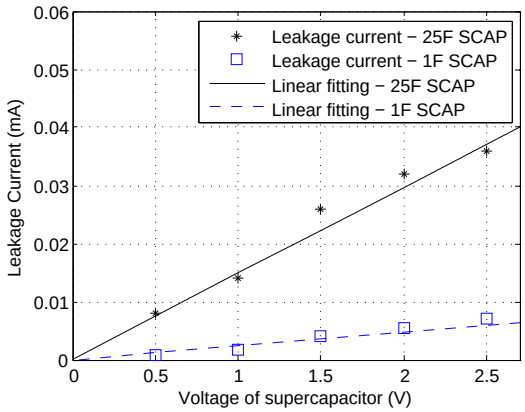

Fig. 1.10 Leakage current vs. voltage of 25 F and 1 F Supercapacitor

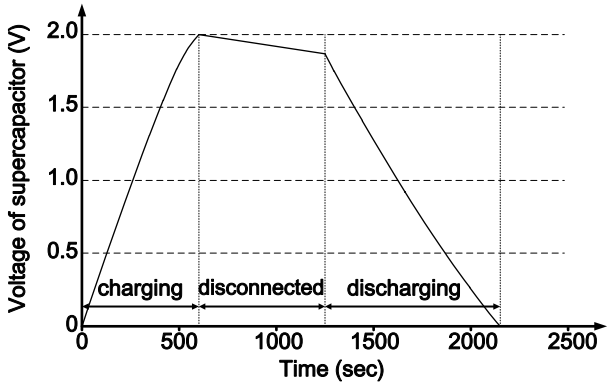

Fig. 1.11 Voltage decreasing during the delay interval

and using 1.12, the $R_{\text{epr,scap}}$ of 25 F and 1 F supercapacitors can be computed as 67.6 kΩ and 312.5 kΩ, respectively.

Charge redistribution: Supercapacitor are made up of two porous electrodes immersed in electrolyte and separated by one porous insulating membrane. Its physical structure increases the farad value as well as the complexity of accurate modeling. They also experience several charge-distribution processes with different time constants, even in isolated and disconnected state. This makes it difficult to identify the process that is responsible for voltage variations. After just being charged for a short period, a disconnected supercapacitor will exhibit a decreasing voltage. This decrease is mainly caused by a charge distribution within branches. In Fig. 9(b), charge redistribution happens when the voltages across C_{sc} (i.e.,$C_{sc} = C_a + C_v$) and C_b do not equal. The dissipated energy due to charge redistribution is mainly consumed by R_2 as long as the charging and discharging current are within a limited

range (< 1 A).

$$P_{\text{redist.}} \approx \frac{(V_{C_{sc}} - V_{C_b})}{R_2} \tag{1.14}$$

From Eq. (1.14), we can see that the larger difference between $V_{C_{sc}}$ and V_{C_b}, the higher charge redistribution power is. Fig. 1.11 illustrates the internal charge-distribution processes of the supercapacitor. For this, a delay period of 10 min was inserted in between the charging and discharging phases of a 22-F supercapacitor. The capacitor was charged from an initial voltage of 12.5 V, and during the delay, the charged supercapacitor was disconnected. An important phenomenon that accounts for the nonideality of the supercapacitor is the decrease of the supercapacitor voltage during the delay interval. No energy is extracted from the supercapacitor, and still, the voltage decreases. This is mainly caused by the charge-distribution process that, in the short term, is more important than leakage.

Unusable residual energy: The unusable energy in the supercapacitor whose voltage is below the minimum dc-dc conversion threshold is called *residual energy*.

E_{residual}: the unusable remaining energy within the supercapacitor.

$$E_{\text{residual}}(t) = \begin{cases} E_{\text{held}}(t) & \text{if } V(t) < V_{\text{conv,min}} \\ \frac{1}{2}C(V_{\text{conv,min}})^2 & \text{if } V(t) \geq V_{\text{conv,min}} \end{cases} \tag{1.15}$$

where $V_{\text{conv,min}}$ is the minimum conversion voltage of a dc-dc converter or a charge pump. The typical $V_{\text{conv,min}} = 0.7$ V, which translates into $E_{\text{residual}} \approx 0.245C$ when the voltage converter is operating.

E_{usable}: the available energy in the supercapacitor for actually driving load.

$$E_{\text{usable}}(t) = E_{\text{held}}(t) - E_{\text{residual}}(t) \tag{1.16}$$

Most commercially available supercapacitors have a voltage range of 0-2.7 V. For a supercapacitor to supply regulated power (typically 3-5 V) to the load, most subwatt-scale harvesters use a boost-up dc-dc converter. However, the minimum voltage of most commercial off-the-shelf dc-dc converters is 0.7 V (e.g., MAX 1763), below which the converter may work in pass-through mode, but the voltage is still too low to drive the typical load. All supercapacitors can withhold up to $\frac{1}{2} \cdot C \cdot (0.7\text{V})^2$ of residual energy. For example, the residual energy of a harvester using a 300 F supercapacitor is up to 73.5 J. Many subwatt-scale harvesters are designed for wireless sensor nodes that consume 100-150 mW while in active mode: e.g., Mica2 at 3.3 V/16 mA; iMote at 2.5 V/60 mA; Eco node at 3.3 V/30.8 mA. This 73.5 J residual energy can operate Eco node (52.8 mW) for 1392 seconds (23 minutes and 12 seconds) in active mode. This is a considerable amount of unusable residual energy.

Size and topology: To address residual energy issue, various reconfigurable supercapacitor topologies are attempted for sustainable operation of the target smart sensing systems. If a single large supercapacitor is employed as the primary en-

ergy buffer (reservoir) for sustained operation, then larger capacitance can cause the longer charging time as well as more unusable residual energy. A related problem is *cold booting* [8], the futile cycles of repeated booting and exhaustion while starting a system with little or no *usable* charge (i.e., near the usable threshold) in the supercapacitor, despite the nontrivial *residual* charge in it. To address the issues with the size constraint of the harvester, the topology of ESE needs to be considered at the system level.

Single Supercapacitor Topology The *single supercapacitor* (SS) topology is the simplest static topology as shown in Fig. 12(a). Systems with a *single small supercapacitor* (SSS, 1-5 F) [26, 42] can charge faster but cannot sustain too many days without sunlight. On the other hand, those with a *single large supercapacitor* (SLS, 50-100 F) [4, 37] have a larger amount of storage energy for sustainable operation, but they may have problems with cold booting and take longer charging time. Furthermore, given the same charging-discharging profile, SLS results in a larger amount of residual energy than SSS does.

Reservoir Supercapacitor Array Topology To address the problems with SS, *reservoir supercapacitors arrays* (RSA) were proposed [6, 30], as shown in Fig. 12(b). The purpose of the topology is to shorten the charging time by replacing an SLS with an array of supercapacitors. Since the leakage rate is dependent on the capacitance of supercapacitors, the RSA topology is also helpful in reducing the leakage rate. However, by charging the reservoir supercapacitors sequentially (e.g., [6]) the RSA topology can result in lower energy efficiency of storage. Because the leakage rate of supercapacitors increases rapidly as they approach their maximum rated voltage, one fully charged reservoir supercapacitor would experience the rapid leakage rate while the other reservoir supercapacitor is being charged. One way to address this problem is to keep the supercapacitors voltage-balanced by either *alternating charging* or charging them *in series* [17].

Dynamic Reconfigurable Supercapacitors According to Fig. 1.10, the leakage current increases as the terminal voltage approaches the maximum rated voltage of the supercapacitor. Particularly, the leakage power near the maximum rated voltage may be as much as 40 times greater than the lowest leakage power. However, this sharp increase of leakage power near the maximum rated voltage is mitigated along with the lower capacitance of supercapacitors. The SS topology does not have any leakage replenishment techniques. The RSA topology has better control because it divides the stored energy of an SLS among several supercapacitors, although the leakage sum does not make a great impact on leakage reduction. To address all these issues, the *dynamic reconfigurable supercapacitors* (DRS) scheme was proposed [16]. During charging and discharging phases, the DRS can be configured for different topologies to control the energy leakage, to reduce the unusable residual energy in the supercapacitors, and to improve output-stage efficiency.

Cold booting: Cold booting, also known as the zero-energy boot-strap problem, is one where the system starts up from nearly fully depleted energy in an energy harvesting system. A system can enter this state after having been deprived of sunlight

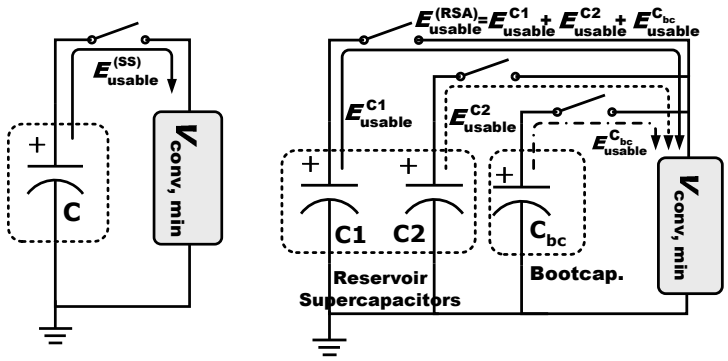

(a) Single Supercapacitor Topology (b) Reservoir Supercapacitor Array Topology

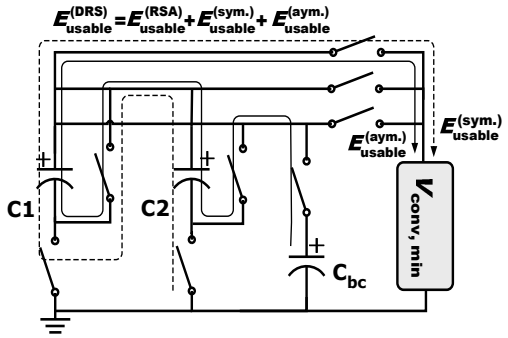

(c) Dynamic Reservoir Supercapacitor Topology

Fig. 1.12 Supercapacitor Topologies for ESE

for an extended period of time and more sunlight is just becoming available. This is problematic, because if the system starts booting as soon as the harvested power exceeds the usable threshold, it is likely to fail if the harvested power does not increase monotonically at a faster rate than the load. The MCU may boot successfully, but any surge due to RF activities can quickly cause any just harvested stored power to be depleted quickly, too, causing the entire system to fail. Such a system is likely to repeat the futile attempt to boot up until sufficient sunlight is available.

The solutions to cold booting be classified into software control, inhibited start by Schmitt trigger, and bootstrap supercapacitor. Ambimax's [30] feedback regulator used for charging the supercapacitor will respond to inrush current by duty cycling it at a very low rate that is incompatible with MPPT. Everlast [37] addresses the inrush current problem by using a feed-forward regulator instead, but it does not inhibit

cold booting. Solar Biscuit [26] and TwinStar [42] use software control and hardware control (Schmitt trigger), respectively, to inhibit futile booting until sufficient energy has been accumulated, but neither performs MPPT, and the inhibiting delay may grow too long for supercapacitors of large capacitance values. DuraCap [6] uses a *bootstrap supercapacitor*, named bootcap (C_{bc}), which has relatively smaller capacitance than the reservoir supercapacitors to solve the cold booting problem by reaching a higher voltage faster with more usable energy for booting. The bootcap has a higher priority to charge, and when it is full, the reservoir ones are charged sequentially (one at a time).

1.5 Summary

Smart sensing systems have been mainly powered by batteries, but supercapacitors are fast becoming a viable alternative form of energy storage for those smart sensing systems that harvest energy for long-term operation. They overcome the 1-2 year service life of batteries and can deliver high current, but their limitations require solutions at not only the circuit level but also the system level. A complete energy-harvesting system includes an energy transducer, energy harvesting circuitry, an energy storage element, and the smart sensing system as the target load. The state-of-the-art in subwatt-scale harvesters can be characterized by their *low overhead* in maximum power point tracking (MPPT) or maximum power transfer tracking (MPTT), and their use of *supercapacitors* as a potential type of energy storage element. For supercapacitors to replace batteries, the harvester must consider leakage, residual energy, topology, energy density, charge redistribution. Thus, this chapter focuses on describing the impact of the nonlinearities of supercapacitors and the way to compensate or overcome these disadvantages at the system and circuit levels.

References

1. Ahska, R., Mamur, H.: A review: Thermoelectric generators in renewable energy. International Journal of Renewable Energy Research (IJRER) 4, 128–136 (2014)
2. Beeby, S., Tudor, M., White, N.: Energy harvesting vibration sources for microsystems applications. Journal of measurement science and technology 17(12), 175–196 (October 2006)
3. Bierschenk, J.: Optimized thermoelectrics for energy harvesting applications. In: Proceedings of the 17th International Symposium on the Applications of Ferroelectrics (ISAF). pp. 1–4. Santa Re, NM, USA (February, 23-28 2008)
4. Brunelli, D., Moser, C., Thiele, L., Benini, L.: Design of a solar-harvesting circuit for batteryless embedded systems. IEEE Transactions on Circuits and Systems 56, 2519–2528 (November 2009)
5. Burke, A.: Ultracapacitors: why, how, and where is the technology. Journal of Power Sources 91, 37–50 (November 2000)
6. Chen, C.Y., Chou, P.H.: DuraCap: a supercapacitor-based, power-bootstrapping, maximum power point tracking energy-harvesting system. In: Proceedings of the International Sympo-

sium on Low Power Electronics and Design (ISLPED). pp. 313–318. ACM, Austin, TX, USA (August 2010)
7. Chevalerias, O., O'Donnell, T., Power, D., O'Donovan, N., Duffy, G., Grant, G., O'Mathuna, S.C.: Inductive telemetry of multiple sensor modules. IEEE Pervasive Computing 4(1), 46–52 (January-March 2005)
8. Chou, P.H., Kim, S.: Techniques for maximizing efficiency of solar energy harvesting systems. In: Proceedings of the Fifth Conference on Mobile Computing and Ubiquitous Networking (ICMU 2010). Seattle, WA, USA (April, 26-28 2010)
9. Chou, P.H., Li, D.: Maximizing efficiency of solar-powered systems by load matching. In: Proceedings of the International Symposium on Low Power Electronics and Design (ISLPED). pp. 162–167 (August, 9-11 2004)
10. Diab, Y., Venet, P., Gualous, H., Rojat, G.: Electrical, frequency and thermal measurement and modelling of supercapacitor performance. In: The 3rd European Symposium on Supercapacitors and Applications. pp. 1066–1069. Rome Italy (November 6-7 2008)
11. Dutta, P., Hui, J., Jeong, J., Kim, S., Sharp, C., Taneja, J., Tolle, G., Whitehouse, K., Culler, D.: Trio: Enabling sustainable and scalable outdoor wireless sensor network deployments. In: The Fifth International Conference on Information Processing in Sensor Networks (IPSN/SPOTS). pp. 407–415 (April, 19-21 2006)
12. Ferrari, M., Ferrari, V., Guizzetti, M., Marioli, D., Taroni, A.: Characterization of thermoelectric modules for powering autonomous sensors. IEEE Transactions on Instrumentation and Measurement 58, 99–107 (May 2009)
13. Hohm, D., Ropp, M.: Comparative study of maximum power point tracking algorithms using an experimental, programmable, maximum power point tracking test bed. In: Conference Record of the Twenty-Eighth IEEE Photovoltaic Specialists Conference. pp. 1699–1702 (September, 15-22 2000)
14. Jiang, X., Polastre, J., Culler, D.: Perpetual environmentally powered sensor networks. In: Proceedings of Fourth International Symposium on Information Processing in Sensor Networks (ISPN). pp. 463–468 (April,15 2005)
15. Kim, R., Lai, J., York, B., Koran, A.: Analysis and design of maximum power point tracking scheme for thermoelectric battery energy storage system. IEEE Transactions on Industrial Electronics 56, 3709–3716 (2009)
16. Kim, S., Chou, P.H.: Energy harvesting by sweeping voltage-escalated charging of a reconfigurable supercapacitor array. In: Proceedings of the International Symposium on Low Power Electronics and Design (ISLPED). pp. 235–240. ACM, Fukuoka, Japan (August 1-3 2011)
17. Kim, S., Chou, P.H.: Size and topology optimization for supercapacitor-based sub-watt energy harvesters. IEEE Transactions on Power Electronics 28, 2068–2080 (April 2013)
18. Kim, S., Torbol, M., Chou, P.H.: Remote structural health monitoring systems for next generation scada. Smart Structures and Systems 11 (May 2013)
19. Kim, Y., Chang, N., Wang, Y., Pedram, M.: Maximum power transfer tracking for a photovoltaic-supercapacitor energy system. In: Proceeding of the 16th ACM/IEEE International Symposium on Low Power Electronics and Design ISLPED. pp. 307–312. ACM, New York, NY, USA (August 2010)
20. KINETRON: The micro generating system for a watch. `http://www.kinetron.eu/wp-content/uploads/2014/04/MGSWatch.pdf`
21. Koutroulis, E., Kalaitzakis, K., Voulgaris, N.: Development of a microcontroller-based, photovoltaic maximum power point tracking control system. IEEE Transactions on Power Electronics 16, 46–54 (January 2001)
22. Koutroulis, E., Kalaitzakis, K.: Design of a maximum power tracking system for wind-energy-conversion applications. IEEE Transactions on Industrial Electronics 53(2), 486–494 (April 2006)
23. Kymissis, J., Kendall, C., Paradiso, J., Gershenfeld., N.: Parasitic power harvesting in shoes. In: Proceedings of the 2nd IEEE International Conference Wearable Computing. pp. 132–139. CA, USA (1998)

24. Kymissis, J., Kendall, C., Paradiso, J.A., Gershenfeld, N.: Parasitic power harvesting in shoes. In: Proceedings of the Second IEEE International Symposium on Wearable Computers (ISWC). pp. 132–139. IEEE Computer Society Washington, DC, USA (1998)
25. Lee, D., Noh, H., Hyun, D., Choy, I.: An improved MPPT converter using current compensation method for small scaled PV-applications. In: The 18th Annual IEEE Applied Power Electronics Conference and Exposition. vol. 1, pp. 540–545 (February, 9-13 2003)
26. Minami, M., Morito, T., Morikawa, H., Aoyama, T.: Solar Biscuit: A battery-less wireless sensor network system for environmental monitoring applications. In: The 2nd International Workshop on Networked Sensing Systems (2005)
27. Noguchi, T., Togashi, S., Nakamoto, R.: Short-current pulse based adaptive maximum-power-point tracking for photovoltaic power generation system. In: Proceedings of 2000 IEEE International Symposium on Industrial Electronics. vol. 1, pp. 157–162 (2000)
28. Ottman, G.K., Hofmann, H.F., Bhatt, A.C., Lesieutre, G.A.: Adaptive piezoelectric energy harvesting circuit for wireless remote power supply. IEEE Transactions on Power Electronics 17, 669–676 (September 2002)
29. Park, C., Chou, P.H.: PUMA: Power utility maximization for multiple-supply systems by a load-matching switch. In: Proceedings of International Symposium on Low Power Electronic Design (ISLPED). pp. 168–173 (August, 9-11 2004)
30. Park, C., Chou, P.H.: AmbiMax: Efficient, autonomous energy harvesting system for multiple-supply wireless sensor nodes. In: Proceedings of 3rd Annual IEEE Communications Society Conference on Sensor, Mesh, and Ad Hoc Communications and Networks (SECON). pp. 168–177 (September, 25-28 2006)
31. Park, C., Chou, P.H.: Eco: Ultra-wearable and expandable wireless sensor platform. In: Proceedings of the third International Workshop on Body Sensor Networks (BSN 2006). pp. 162–165. IEEE Computer Society Washington, DC, USA, MIT Media Lab, USA (April, 3-5 2006)
32. Park, C., No, K., Chou, P.H.: TurboCap: Batteryless, supercapacitor-based power supply for Mini-FDPM. In: Proceedings of 3rd European Symposium on Supercapacitors and Applications (ESSCAP). Rome, Italy (November 2008)
33. Petreus, D., Moga, D., Galatus, R., Munteanu, R.A.: Modeling and sizing of supercapacitors. Advances in Electrical and Computer Engineering 8(2), 15–22 (November 2008)
34. Raghunathan, V., Kansal, A., Hsu, J., Friedman, J., Srivastava, M.: Design considerations for solar energy harvesting wireless embedded systems. In: Proceedings of the 4th international Symposium on Information Processing in Sensor Networks (IPSN). pp. 457–462 (April 25-27 2005)
35. Roundy, S., Wright, P.: A piezoelectric vibration based generator for wireless electronics. Journal of Smart Materials and Structures 13(5), 1131–1142 (2004)
36. Sera, D., Teodorescu, R., Rodriguez, P.: PV panel model based on datasheet values. In: IEEE International Symposium on Industrial Electronics (ISIE). pp. 2392–2396 (June, 4-7 2007)
37. Simjee, F., Chou, P.H.: Efficient charging of supercapacitors for extended lifetime of wireless sensor nodes. IEEE Transactions on Power Electronics 23, 1526–1536 (May 2008)
38. Williams, C., Yates, R.: Analysis of a micro-electric generator for microsystems. In: Proceedings of Eurosensors. pp. 369–372 (1995)
39. Xiao, W., Dunford, W.: A modified adaptive hill climbing MPPT method for photovoltaic power systems. In: 2004 35th Annual IEEE Power Electronics Specialists Conference. vol. 3, pp. 1957–1963 (June, 20-25 2004)
40. Yang, H., Zhang, Y.: Analysis of supercapacitor energy loss for power management in environmentally powered wireless sensor nodes. IEEE Transaction on Power Electronics 28(11), 5391–5403 (November 2013)
41. Zhu, G.R., Loo, K.H., Lai, Y.M., Tse, C.K.: Quasi-maximum efficiency point tracking for direct methanol fuel cell in DMFC/supercapacitor hybrid energy system. IEEE Transaction on Energy Conversion 27(3), 561–571 (Septemper 2012)
42. Zhu, T., Zhong, Z., Gu, Y., He, T., Zhang, Z.L.: Leakage-aware energy synchronization for wireless sensor networks. In: The 8th Annual International Conference on Mobile Systems, Applications, and Services (MobiSys) (June 15-18 2010)